

Graphene superlattice with periodically modulated Dirac gap

G.M. Maksimova, E.S. Azarova, A.V. Telezhnikov, and V.A. Burdov
*Department of Theoretical Physics, University of Nizhny Novgorod,
23 Gagarin Avenue, 603950 Nizhny Novgorod, Russian Federation*
(Dated: August 8, 2018)

Graphene-based superlattice (SL) formed by a periodic gap modulation is studied theoretically using a Dirac-type Hamiltonian. Analyzing the dispersion relation we have found that new Dirac points arise in the electronic spectrum under certain conditions. As a result, the gap between conduction and valence minibands disappears. The expressions for the positions of these Dirac points in \mathbf{k} -space and threshold value of the potential for their emergence were obtained. Also, the dispersion law and renormalized group velocities around the new Dirac points were calculated. At some parameters of the system, we have revealed interface states which form the top of the valence miniband.

PACS numbers: 71.10.Pm, 73.21.-b, 81.05.U-

I. INTRODUCTION

During for the last years extremely much attention was paid to the electronic properties of graphene (see Ref.1 for the review). Such interest results, in particular, from the fact that physics of the low-energy carriers in graphene is governed by a Dirac-type Hamiltonian. The band structure of an ideal graphene sheet has no energy gap. As a consequence, Dirac electrons become massless, and reveal unusual properties such as perfect transmission at normal incidence through any potential barrier (the Klein paradox^{2,3}), trembling motion (or Zitterbewegung⁴), etc. Because of the Klein effect, an electrostatic potential cannot confine electrons in graphene. This property of graphene impedes its use in electronic devices.⁵ However, as has been shown,⁶ it is possible to confine massless Dirac particle in graphene sheet by inhomogeneous magnetic field. The confinement can be also achieved by combining electric and uniform magnetic fields.^{7,8} Meanwhile, Dirac electrons can be localized electrostatically in a gapped graphene.

The gap can be induced by substrate or strain engineering as well as by deposition or adsorption of molecules on a graphene layer. For example, two carbon sublattices of graphene placed on top of hexagonal boron nitride (h -BN) become nonequivalent due to their interaction with the substrate. The band-structure calculations within the local-density approximation for this system gives a gap not less than 53 meV.⁹ A hydrogenated sheet of graphene (graphane) is a semiconductor with a gap of the order of a few eV.¹⁰

Besides, it is possible to modulate spatially the gap (i.e. the particle's mass) in graphene. It was shown that the spatial mass dependence leads to suppression of Klein tunneling and induces confined states.^{11,12} The required gap modulation can be created, for instance, in graphene placed on a substrate fabricated from different dielectrics. It is also possible to use for this purpose an inhomogeneously hydrogenated graphene or graphene sheet with nonuniformly deposited CrO_3 molecules. Correspondingly, one can fabricate different graphene het-

erostructures with the gap discontinuity. In particular, graphene-based superlattice (SL) can be formed due to the periodic modulation of the band gap.

Recently, electronic structure of graphene under external periodic potential has been the subject of numerous studies.¹³⁻²⁸ Increasing interest in graphene SLs results from the prediction of possible engineering the system band structure by the periodic potential, which opens new ways for fabrication of graphene-based electronic devices. The graphene SLs have been realized experimentally. For example, graphenes grown epitaxially on metal surfaces²⁴⁻²⁷ demonstrate SL patterns with about several nanometers SL period. Recent scanning tunneling microscopy studies²⁸ of corrugated graphene monolayer on Rh foil show that the quasi-periodic ripples generate a weak one-dimensional electronic potential in graphene leading to emergence of the SL Dirac points. It was as well shown theoretically that a one-dimensional periodic potential really affects the transport properties of graphene. For instance, the Kronig-Penney (KP)-type electrostatic potential induces strong anisotropy in the carrier group velocity around the Dirac point^{13,17} leading to the so-called supercollimation phenomenon.^{13,14} Besides, in the SL spectrum new (extra) Dirac points appear in Brillouin zone. These features has been also examined for the different types of graphene SL including the magnetic KP-SL with delta-function magnetic barriers.¹⁸⁻²³ In Ref.19 the first-principles studies of the electronic structure of graphene-graphene SL modeled with a repeated structure of pure and hydrogenated graphene (i.e., graphane) strips has been performed. It was found that unlike other graphene nanostructures, the hydrogenated graphene SLs exhibit both direct and indirect band gaps.

In this paper we focus on the electronic states in graphene-based SL with periodically modulated gap and relative band shift (potential) where the gap and potential are piecewise constant functions of x . The model of such SL has been considered earlier.²⁹ However, no detailed examination of the electronic structure in such type SLs in a wide range of the system parameters has been carried out. In particular, we have first found that

the considered SL can be gapped or gapless depending on the band shift. We analyze in detail the SL with equal widths of the gapless and gapped graphene fractions, and show that the forbidden miniband exists up to some threshold value $V = V_c$ corresponding to the first emergence of the Dirac-like point at $\mathbf{k} = 0$. When the potential V exceeds V_c , this Dirac-like point disappears, opening the minigap at $\mathbf{k} = 0$. At the same time, two extra Dirac points arise in symmetric positions on the k_y axis. This scenario differs from the one realized in graphene SL formed by the electrostatic potential,¹⁷ where the original Dirac point (at $\mathbf{k} = 0$) always exists. Further V increasing leads to emergence of a new pair of the Dirac points from the origin $\mathbf{k} = 0$. The dispersion in the vicinity of these points appears to be anisotropic, indicating an anisotropic renormalization of the group velocity. We also show that interface states can exist in the gap-induced SL in contrast to the SL formed by a Kronig-Penney-type electrostatic potential. For this case the relevant conditions and values of the system parameters were obtained.

II. DIRAC PARTICLE IN GRAPHENE SUPERLATTICE

Let us consider one-dimensional (1D) graphene superlattice with period l formed by position-dependent gap and band shift. As was shown in Ref.29, such structure can be realized, e.g., on the base of graphene deposited on a strip substrate combined from silicon oxide and h -BN (Fig.1). The SL electronic structure in the vicinity of \mathbf{K} -point of the Brillouin zone is described by the Dirac-like Hamiltonian

$$\hat{H} = v_F \hat{\mathbf{p}} \hat{\boldsymbol{\sigma}} + V(x) \hat{1} + \Delta(x) \hat{\sigma}_z \quad (1)$$

where $\hat{\mathbf{p}}$ is the momentum operator, $\hat{\sigma}_i$ are the Pauli matrices, $\hat{1}$ is a unit 2×2 matrix, v_F is the Fermi velocity, and $\Delta(x)$, $V(x)$ are periodic functions equal to Δ and V , respectively, at $a \leq x \leq l$, and zero at $0 \leq x < a$. Here, the potential V defines the shift of the forbidden band center in the gapped graphene with respect to the Dirac point in the gapless graphene^{29,30} (see Fig.1). Generally speaking, the Fermi velocity can differ in graphene modifications placed on different substrates. In our model, however, we neglect the dependence v_F on x supposing $v_F \approx 10^8$ cm/s in both graphene fractions.

The Kronig-Penney model considered here as applied to graphene SL is also used in many other physical problems including, e.g., modeling of semiconductor SLs or relativistic particle dynamics. Although master equations describing the single-particle evolution differ for all the mentioned systems, explicit forms of the dispersion relations obtained within the framework of the Kronig-Penney model resemble to each other. Nevertheless, individual features of these systems result in qualitative distinctions in their band structures. For instance, the

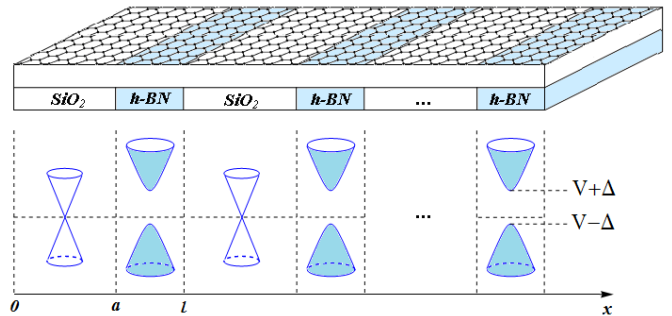


FIG. 1: (Color online) Top: graphene layer on the striped substrate composed of silicon oxide and hexagonal boron nitride. Bottom: schematic diagram showing the electronic energy spectrum in graphene SL.

dispersion relation for 1D relativistic electron in Kronig-Penney potential^{31,32} is similar to the one obtained in this paper (see Eq.(9) below) for 2D electrons in 1D graphene SL. In our case, however, the periodic potential in Dirac-like equation is formed by two terms having different meanings from the point of view of relativistic physics. The relative band shift V can be treated as the time-like vector component while the band-gap Δ represents a scalar potential. This circumstance together with the two-dimensionality of the electron gas provide new fundamental properties of the SL electronic structure (such as appearance of extra Dirac points), which will be discussed in detail in section III.

The Dirac equation

$$\hat{H}\Psi(x, y) = E\Psi(x, y) \quad (2)$$

admits the solutions $\Psi(x, y) = \exp(ik_y y)\Psi(x)$, where the two-component spinor envelope function $\Psi(x)$ satisfies the equation

$$i \frac{d\Psi}{dx} = \hat{h}(x)\Psi(x) \quad (3)$$

with

$$\hat{h}(x) = \begin{pmatrix} ik_y & \frac{V(x)-E-\Delta(x)}{\hbar v_F} \\ \frac{V(x)-E+\Delta(x)}{\hbar v_F} & -ik_y \end{pmatrix}. \quad (4)$$

The formal solution of Eq.(3) is

$$\Psi(x) = \hat{\mathfrak{R}}_x \exp\left(-i \int_{x_0}^x \hat{h}(x_1) dx_1\right) \Psi(x_0), \quad (5)$$

where $\hat{\mathfrak{R}}_x$ is the spatial ordering operator.^{32,33} This expression can be simplified as

$$\Psi(x) = \exp(-i(x-x_0)\hat{h})\Psi(x_0) \quad (6)$$

if both points x and x_0 belong to the space-homogeneous region.

In this case it is convenient to define the matrix

$$\hat{t}(x - x_0) = \exp(-i(x - x_0)\hat{h}). \quad (7)$$

Here, the matrix \hat{h} is defined by Eq.(4) where $V(x) = \Delta(x) = 0$ if $0 \leq x, x_0 < a$, and $V(x) = V, \Delta(x) = \Delta$ if $a \leq x, x_0 \leq l$. The straightforward calculation yields $\hat{h}^2(x) = K^2(x)\hat{1}$, where $K(x) = \sqrt{((V(x) - E)^2 - \Delta^2(x))/(\hbar v_F)^2 - k_y^2)}$. Therefore, all even powers in the Taylor series of the exponential function in Eq.(7) will be proportional to the unit matrix while all odd powers will be proportional to the matrix \hat{h} itself. This leads to the following expression:

$$\hat{t}(x - x_0) = \hat{1} \cos \alpha - i\hat{h}(x) \frac{\sin \alpha}{K(x)} = \begin{pmatrix} \cos \alpha + \frac{k_y}{K(x)} \sin \alpha & -i \sin \alpha \frac{V(x) - E - \Delta(x)}{\hbar v_F K(x)} \\ -i \sin \alpha \frac{V(x) - E + \Delta(x)}{\hbar v_F K(x)} & \cos \alpha - \frac{k_y}{K(x)} \sin \alpha \end{pmatrix}, \quad (8)$$

where $\alpha = (x - x_0)K(x)$.

We can now find that $\Psi(l) = \hat{T}\Psi(0)$, where $\hat{T} = \hat{t}(l - a)\hat{t}(a)$. Note, that $\det(t) = 1$, and, consequently, $\det(T) = 1$ as well. This equality and the Bloch condition $\Psi(l) = \Psi(0) \exp(ikl)$ (here, k is the Bloch wave vector) yield the dispersion relation $2 \cos(kl) = \text{Tr}(T)$ for the 1D graphene-based SL. Using Eq.(8) one can find $\text{Tr}(T) = \text{Tr}(t(l - a)t(a))$. Accordingly, the resulting dispersion equation reads

$$\cos(kl) = \cos(k_x a) \cos(q_x(l - a)) + \frac{EV - (\hbar v_F k_x)^2}{(\hbar v_F)^2 k_x q_x} \sin(k_x a) \sin(q_x(l - a)), \quad (9)$$

with $k_x \equiv K(+0)$, $q_x \equiv K(l - 0)$. At $(V - E)^2 - \Delta^2 < (\hbar v_F k_y)^2$, the wave number q_x is imaginary and the allowed energies are given by Eq.(9) with q_x replaced by $i|q_x|$.

Eq.(9) for the allowed energies was obtained also in Ref.29 via wave function matching. However some results of this work concerning the miniband structure and existence of the interface states seem questionable. Below we discuss these issues in detail. Note that at $\Delta = 0$, Eq.(9) coincides with the one found for single-layer graphene in a periodic piecewise constant potential $V(x)$.^{17,33,34}

III. ELECTRONIC STRUCTURE

The miniband structure depends on the system parameters as well as on the y -component of the wave vector. As seen from the Eq.(9), the dispersion relation is invariant with respect to the simultaneous replacements $E \rightarrow -E, V \rightarrow -V$. Therefore, in what follows we shall consider, for definiteness, only nonnegative values of the relative band shift: $V \geq 0$. When $V = 0$, the energy spectrum is completely symmetric related to the value $E = 0$ corresponding to the original Dirac point in the

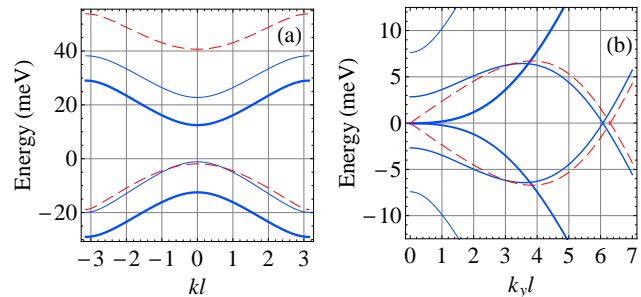


FIG. 2: (Color online) (a). Two low-energy minibands of the SL spectrum with $k_y = 0, l = 60$ nm, and $\Delta = 26.5$ meV. Thick (blue) line corresponds to the band shift $V = 0$, and $a = l/2$. Thin (blue) and dashed (red) lines correspond to the widths of gapless graphene fraction $a = l/2$ and $a = l/6$, respectively, at $V = 24.2$ meV. (b). k_y -dependence of the electron energies in the conduction and valence minibands at $k = 0, l = 60$ nm, $a = l/2, \Delta = 0$, and $V = 195.7$ meV (dashed red line). For other curves $\Delta = 26.5$ meV and $V = 77.1$ meV (thin blue solid line); $V = 143.26$ meV (thick blue solid line), and $V = 195.7$ meV (solid blue line). The zeroth energy corresponds to the minigap center for thin solid line, and to the contact and cone-like Dirac points for all the others.

gapless graphene. In this case the two first minibands symmetrically situated above and below the point $E = 0$ are the conduction and valence ones, respectively. As V increases, the conduction and valence minibands gradually shift up. Below we shall concentrate on these two minibands only, assuming the Fermi level to be in between at any V .

The electron and hole energies as functions of k at $k_y = 0, \Delta = 26.5$ meV for different values of the potential V and widths a are plotted in Fig.2(a). The parameters we choose are appropriate for graphene. Thick and thin solid lines correspond to $V = 0$ and $V = 24.2$ meV, respectively, and $a = l/2$. When V becomes nonzero the electron (conduction) and hole (valence) minibands shift up, and the electron miniband turns out to be a little narrower than the hole one. This is, presumably, due to the fact that at chosen values of the parameters the electron miniband completely forms under the barrier at $a < x < l: V - \Delta < E < V + \Delta$, while the hole-miniband energies mainly belong to the over-barrier region $E < V - \Delta$.

The energy branches in the conduction and valence minibands at $a = l/6, V = 24.2$ meV is shown with dashed line. We can see that, as the gapped graphene fraction in the SL increases, the electron-hole minigap increases too. Nevertheless, in any case, at $k_y = 0$ the minigap cannot exceed the gap value 2Δ .³⁵ Indeed, it is clear that if the whole graphene layer is gapped, i.e. $a = 0$, the forbidden miniband should be 2Δ (at $k_y = 0$).

Figure 2(b) illustrates the dependence of the electron and hole energies on k_y at different V and Δ , and $k = 0, a = l/2, l = 60$ nm. We show only semiaxis $k_y > 0$ be-

cause of the symmetry $k_y \rightarrow -k_y$ in the dispersion law [Eq.(9)]. The energies in the figure are counted from the minigap center (its position determined at $k = k_y = 0$ depends on V) for $V = 77.1$ meV (thin solid line) at $\Delta = 26.5$ meV. In other cases the energy origin coincides with the contact or cone-like point energy. Our calculations demonstrate a monotonous expansion of the forbidden miniband with $|k_y|$ increasing (thin solid line in Fig.2(b)) until V becomes greater than some threshold value V_c (for chosen set of parameters $V_c = 143.26$ meV). When $V = V_c$ (thick solid line in Fig.2(b)), the electron and hole energy branches touch each other at $k = k_y = 0$ closing the minigap. When V exceeds V_c , the minigap at $k = k_y = 0$ opens, but two extra Dirac points appear in symmetric positions on the k_y -axis (solid line in Fig.2(b)), and never then vanish. Thus, beginning with $V = V_c$ the gap-induced SL becomes gapless.

This feature of the theoretically predicted dependence of the SL minigap on V , in fact, can be observed by spectroscopic methods. In order to vary the parameter V it is possible to apply additional nano-gate potential to the gapped graphene fractions in the SL. Closing the minigap accompanied by the disappearance of the absorption edge and appearance of the contact point in the SL spectrum allows one, in turn, to determine experimentally the threshold value $V = V_c$.

Further increase of V results in formation of new additional cone-like Dirac points which originate from $k_y = 0$. Such a behavior is not unique. As was shown in Refs 15-17 for gapless graphene, the new Dirac points can emerge in the presence of a sinusoidal or squarewell SL potential. A simple analytical expression for the positions of these points in \mathbf{k} -space has been obtained by different research groups.^{17,33} In our model, however, in contrast to the SLs discussed in the works quoted above, the Dirac point being a prototype of the original Dirac point at $\mathbf{k} = 0$ arises at certain finite values of V equal to $V_n = 2\pi n \hbar v_F / l + \sqrt{(2\pi n \hbar v_F / l)^2 + \Delta^2}$ (defined by the zeroes of k_{yn} , see Eq.(12) below) with n being positive integer. Note that, V_1 coincides with the threshold potential value V_c .

It is clearly seen from Fig.2(b) that extra Dirac point located at $k_{yl} \simeq 6.3$ for $\Delta = 0$ (dashed line) remains also in the case $\Delta \neq 0$ at the same values of V when $\Delta \ll V$. However, the location of the Dirac point in this case slightly shifts towards zero with Δ increasing. In order to find the location of the Dirac points in \mathbf{k} -space we note that $k_x(E, k_y)$ and $q_x(E, k_y)$ coincide at

$$E_0(V) = \frac{V^2 - \Delta^2}{2V}. \quad (10)$$

Correspondingly, Eq.(9) at $a = l/2$, $k = 0$ and $E = E_0$ turns into

$$1 = \cos^2 \frac{k_x l}{2} + \frac{E_0 V - E_0^2 + \hbar^2 v_F^2 k_y^2}{(\hbar v_F k_x)^2} \sin^2 \frac{k_x l}{2}. \quad (11)$$

Obviously this equation is satisfied if $k_x l = 2\pi n$ (n is integer and differs from zero), which leads to $k_y = k_{yn}$,

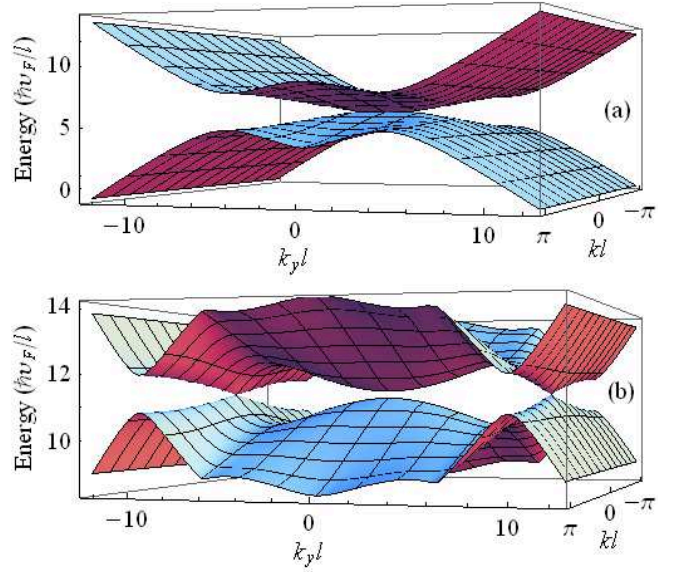


FIG. 3: (Color online) Energy surfaces near the: contact point $k = k_y = 0$ at $V = V_c = 143.26$ meV (a); cone-like Dirac point $k = 0$, $k_y = k_{y1}$ at $V = 165.15$ meV (b). $\Delta = 26.5$ meV.

where

$$k_{yn} = \frac{1}{l} \sqrt{\left(\frac{E_0 l}{\hbar v_F}\right)^2 - (2\pi n)^2}. \quad (12)$$

One can check that for $a = l/2$, the right side of Eq.(9) has local maximum (equal to unity) at $E = E_0$ and $k_y = k_{yn}$. This means coincidence of conduction and valence miniband edges.

According to Eq.(12), in general case, when the ratio $E_0 l / 2\pi \hbar v_F$ is not integer, the number of Dirac points N_D symmetrically situated around $k_y = 0$ is given by

$$N_D = 2 \left[\frac{E_0 l}{2\pi \hbar v_F} \right], \quad (13)$$

where $[...]$ denotes an integer part. One of the contact points is always located at $k_y = 0$ if $E_0 l / \hbar v_F = 2\pi n$. In this case $V = V_n$, and the total number of Dirac points is odd: $N_D = 2n - 1$.

Thus, now we can write analytically the inequality for the system parameters corresponding to the formation of the gapless SL. Evidently, the gap separating the conduction and valence minibands vanishes if

$$\frac{(V^2 - \Delta^2)l}{4\pi \hbar v_F V} \geq 1. \quad (14)$$

The case of the rigorous equality in Eq.(14) corresponds to the threshold value of the potential: $V_c = V_1 = 2\pi \hbar v_F / l + \sqrt{(2\pi \hbar v_F / l)^2 + \Delta^2}$ (the positive root of the quadratic equation).

Solving Eq.(9) numerically we have found the dispersion law presented in Fig.3 for $V = V_1 = V_c$ (panel (a))

and $V_1 < V < V_2$ (panel (b)). It is seen that when $V = V_c$ there is the only contact point in the electronic spectrum, having no conical shape. When $V > V_c$, two cone-like Dirac points exist at $E = E_0(V)$, $k = 0$, and $k_y = \pm k_{y1}$. Let us further consider the dispersion relation in the nearest vicinity of the contact and cone-like Dirac points.

We start with the contact point arising at $E = E_0(V_n)$, $k = 0$, and $k_y = 0$. For this purpose one has to expand the terms in Eq.(9) at $V = V_n$ into the Taylor series up to the lowest powers of $E - E_0(V_n)$, k , and k_y^2 . As an example, below we consider the case $n = 1$, i.e. $V = V_c$. After some algebra one obtains the dispersion relation in the following form:

$$\varepsilon = \frac{d^4(k_y l)^2}{4\pi u_c^2(1 + 3d^2)} \pm \sqrt{\frac{(kl)^2}{1 + 3d^2} + \frac{1 + 3d^2 + d^6/u_c^3}{(1 + 3d^2)^2} \frac{d^2(k_y l)^4}{(4\pi)^2 u_c}}, \quad (15)$$

where we have introduced dimensionless energy $\varepsilon = (E - E_0)l/\hbar v_F$, and parameters $u_c = lV_c/4\pi\hbar v_F$ and $d = l\Delta/4\pi\hbar v_F$. The signs "+" and "-" correspond to the electrons and holes, respectively. Evidently, the energy surface $\varepsilon(k, k_y)$ around the only contact point, indeed, has no conical form. The first term in the right side of Eq.(15) defines an asymmetry of the conduction and valence minibands related to $\varepsilon = 0$. If $d \rightarrow 0$ (in this case $u_c \rightarrow 1$), the conduction and valence minibands become symmetric near the contact point. According to Eq.(15) at $k = 0$, the edges of the conduction and valence minibands are parabolic along k_y -axis:

$$\varepsilon \sim d \left(\frac{d^3}{u_c^{3/2}} \pm \sqrt{1 + 3d^2 + \frac{d^6}{u_c^3}} \right) k_y^2. \quad (16)$$

As a result, the dispersion along k_y is almost flat. In the limiting case $d \ll 1$, the coefficient before k_y^2 becomes proportional to d (i.e. Δ). Note that in the SL based on a gapless graphene the dispersion curves at $k = 0$ also demonstrate a nonlinear behavior, where, however, dispersion is defined by the third power of the y -component of the wave vector: $\varepsilon \sim \pm k_y^3$.¹⁷

Basing on Eq.(15) we can now determine the velocity components $v_k = \hbar^{-1}\partial E/\partial k$, $v_y = \hbar^{-1}\partial E/\partial k_y$ in the vicinity of the contact point at $V = V_c$. Calculating the derivatives one gets

$$\frac{v_k}{v_F} = \pm \frac{k}{\sqrt{(1 + 3d^2)k^2 + \left(1 + 3d^2 + \frac{d^6}{u_c^3}\right) \frac{l^2 d^2 k_y^4}{(4\pi)^2 u_c}}}, \quad (17)$$

$$\frac{v_y}{v_F} = \frac{ld^4 k_y}{2\pi u_c^2(1 + 3d^2)} \pm \frac{\left(1 + \frac{d^6}{(1 + 3d^2)u_c^3}\right) \frac{2l^2 d^2}{(4\pi)^2 u_c} k_y^3}{\sqrt{(1 + 3d^2)k^2 + \left(1 + 3d^2 + \frac{d^6}{u_c^3}\right) \frac{l^2 d^2 k_y^4}{(4\pi)^2 u_c}}}. \quad (18)$$

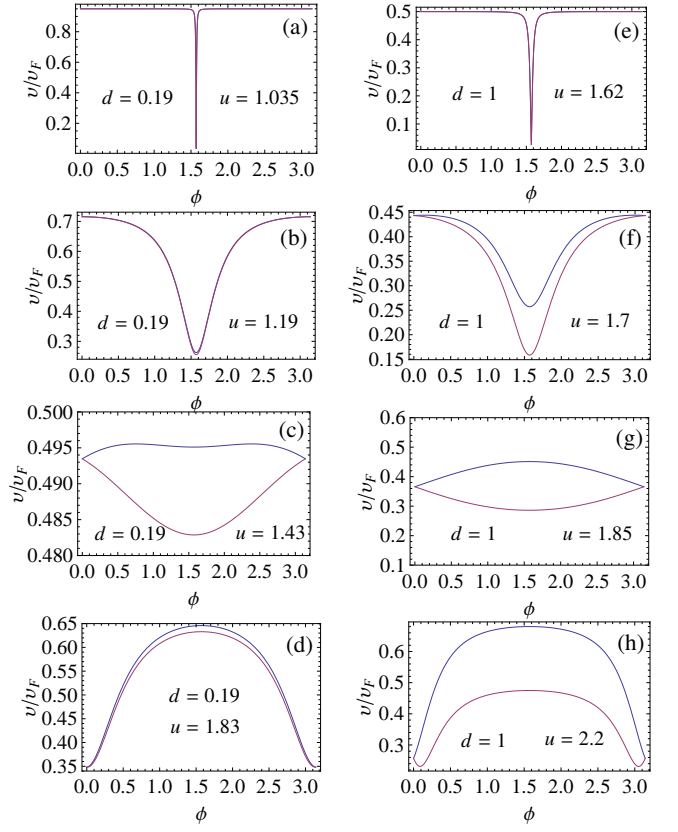


FIG. 4: (Color online) Angle dependence of the absolute value of the electron and hole (upper and lower curves, respectively, in each panel) velocities normalized to v_F near the contact point $k = k_y = 0$ at $Ql = 0.5$, and $V = V_c$ (panels (a) and (e)), and near the cone-like Dirac point $k = 0$, $k_y = k_{y1}$ (panels (b) - (d) and (f) - (h)). Values of d and u are indicated in the figure.

The obtained expressions exhibit strong anisotropy of the electron and hole velocities in (k, k_y) -plane, which is clearly seen from the dependence of the absolute value $v = \sqrt{v_k^2 + v_y^2}$ on the polar angle ϕ introduced with standard relations: $k = Q \cos \phi$, $k_y = Q \sin \phi$, where $Q = \sqrt{k^2 + k_y^2}$. The dependence $v(\phi)$ is sensitive to the induced gap Δ (or d) as Fig.4 shows. When $d \ll 1$ (panel (a)), v is close to v_F for all angles except for the nearest vicinity of $\pi/2$ where narrow dip in the dependence $v(\phi)$ occurs. As d increases, v monotonously decreases in whole, keeping the dip that becomes a little wider as seen in panel (e). Such a dip is caused by the lens-like shape of the energy surfaces $\varepsilon(k, k_y)$ both for the electrons and holes as described by Eq.(15). In this case, the component v_k is much greater than v_y for all ϕ except for the narrow domain near the "lens" edge, where ϕ is close to $\pi/2$. Within this domain both v_k and v_y are small as follows from Eqs (17) and (18). Note also that, the electron and hole velocities v_e and v_h , in fact, coincide at the considered values of d .

Finalizing discussion of the energies and group velocities near the contact point we would like to emphasize as well that, expressions similar to Eqs (15) - (18) can be easily obtained for $V = V_n$. In this case one should simply replace π by πn in all the expressions. Consequently, the dispersion in k_y direction flattens compared to the one described by the Eq.(16).

When $E_0 l / \hbar v_F > 2\pi n$, which implies that $V > V_n$, the situation is different. In this case introducing small deviation $\tilde{k}_y = k_y - k_{yn}$, it is easy to find from Eq.(9) the dispersion law $\varepsilon(k, \tilde{k}_y)$ in the form:

$$\varepsilon = \beta \tilde{k}_y l \pm \sqrt{\alpha^2 (kl)^2 + (\beta^2 + \gamma^2) (\tilde{k}_y l)^2}. \quad (19)$$

Here, the parameters α , β , and γ are defined as

$$\begin{aligned} \alpha &= \frac{un^2}{\sqrt{(u^2 - d^2)^2 (u^2 + d^2) + n^2 d^4}}, \\ \beta &= \frac{d^2 (u^2 - d^2 - n^2) \sqrt{(u^2 - d^2)^2 - u^2 n^2}}{(u^2 - d^2)^2 (u^2 + d^2) + n^2 d^4}, \\ \gamma &= \sqrt{\frac{((u^2 - d^2)^2 - u^2 n^2) (u^2 - d^2 - n^2)}{(u^2 - d^2)^2 (u^2 + d^2) + n^2 d^4}}, \end{aligned} \quad (20)$$

where the dimensionless potential $u = lV/4\pi\hbar v_F$ is always greater than n if $\Delta \neq 0$.

Provided that V slightly exceeds V_n ($V - V_n \ll V_{n+1} - V_n$), the energy surface becomes a cone elongated in k_y -direction. As V increases, the cone gradually turns into the isotropic one, and then becomes elongated in k -direction. Thus, the dispersion law around the new cone-like Dirac points in the considered SL has strong anisotropy dependent on V in contrast to the original Dirac point in a gapless graphene. Similar behavior takes place in the graphene SL formed by V -modulation at $\Delta = 0$.¹⁷ In our case, however, in contrast to the mentioned work, the cone is always tilted due to the presence of the linear in \tilde{k}_y term in the dispersion relation [Eq.(19)]. The cone-axis obliquity is defined by the coefficient β which tends to zero when $\Delta \rightarrow 0$.

The anisotropy of the dispersion law naturally manifests itself in the dependencies of the electron and hole velocities on ϕ . Because of the cone-type shape of the energy surface, the velocity components

$$\begin{aligned} \frac{v_k}{v_F} &= \pm \frac{\alpha^2 \cos \phi}{\sqrt{\alpha^2 \cos^2 \phi + (\beta^2 + \gamma^2) \sin^2 \phi}}, \\ \frac{v_y}{v_F} &= \beta \pm \frac{(\beta^2 + \gamma^2) \sin \phi}{\sqrt{\alpha^2 \cos^2 \phi + (\beta^2 + \gamma^2) \sin^2 \phi}}, \end{aligned} \quad (21)$$

do not depend on Q but exclusively on ϕ . Due to the cone tilt, v_y -component has nonzero mean value

$$\langle v_y \rangle_\phi = \beta v_F \quad (22)$$

being the same for the electrons and holes.

In Fig.4 we have plotted the relation v/v_F around the cone-like Dirac point with $k_y = k_{y1}$ for the electrons and holes as function of the polar angle ϕ for various $V > V_c(\Delta)$ ($u > u_c(d)$) at two values of the gap: $\Delta = 26.5$ meV ($d = 0.19$, panels (b) - (d)), and $\Delta = 138.36$ meV ($d = 1$, panels (f) - (h)). Provided that $d \ll 1$ the parameter β is close to zero, and the Dirac-cone tilt is negligibly small. As a result, v_e and v_h differ insignificantly. The electron and hole velocities vary strongly when α^2 strongly differ from $\beta^2 + \gamma^2$ (panels (b) and (d), where V equals 165.15 meV and 253.23 meV, respectively). This corresponds to the Dirac cone elongated in k_y -direction if $\alpha^2 > \beta^2 + \gamma^2$ (panel (b)) or in k -direction in the opposite case (panel (d)). When $\alpha^2 \approx \beta^2 + \gamma^2$ (this is so, e.g., at $V = 196$ meV) the cone becomes almost isotropic. Consequently, v_e and v_h remain almost constant and equal to $v_F/2$ (panel (c)). At greater d the cone tilt differently influences v_e and v_h , as shown in panels (f) - (h), where V equals 235.2 meV, 256 meV, and 304.4 meV, respectively. The behavior of the electron and hole velocities in this case is qualitatively similar to that takes place at $d \ll 1$. However the difference $v_e - v_h$ is no longer small.

We do not discuss here the case $a \neq l/2$. We expect that Dirac points appear in this case too. However, the electron-hole miniband profile should be significantly asymmetric related to the Fermi level as it was in V -modulated SL.¹⁷

IV. INTERFACE STATES

As was shown by Ratnikov and Silin³⁶ interface states can exist in graphene-based heterojunctions. It was found that interface states result from the crossing of dispersion curves of gapless and gapped graphene modifications. Meanwhile, in graphene-based superlattices, formation of interface minibands was considered to be impossible.²⁹ In contrast to this statement we have found that the interface states can arise under certain conditions discussed below. Since the wave functions of these states behave as exponentials along x -axis, the wave vectors k_x and q_x should be imaginary, so that

$$(\hbar v_F k_y)^2 > E^2, \quad (\hbar v_F k_y)^2 + \Delta^2 > (E - V)^2. \quad (23)$$

In this case Eq.(9) transforms into

$$\begin{aligned} \cos(kl) &= \cosh(k'_x a) \cosh(q'_x (l - a)) + \\ &\frac{EV - E^2 + (\hbar v_F k_y)^2}{(\hbar v_F)^2 k'_x q'_x} \sinh(k'_x a) \sinh(q'_x (l - a)), \end{aligned} \quad (24)$$

with $k'_x = \sqrt{k_y^2 - \frac{E^2}{(\hbar v_F)^2}}$, $q'_x = \sqrt{k_y^2 + \frac{\Delta^2 - (V - E)^2}{(\hbar v_F)^2}}$.

Evidently the solution of this equation can exist only if

$$(\hbar v_F k_y)^2 - E^2 < -EV. \quad (25)$$

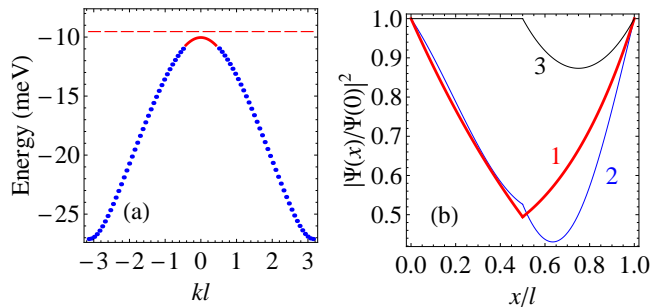


FIG. 5: (Color online) (a). Hole miniband of the SL spectrum for $a = l/2 = 30$ nm, $V = 11$ meV, $\Delta = 22$ meV, and $k_y l = 1$. Top of the energy miniband depicted by the solid (red) line corresponds to the interface states. Dashed (red) line shows the interface energy level for an isolated heterojunction. (b). Probability densities for: interface hole state (both k'_x and q'_x are real) with $k_y l = 1$, $kl = 0.1$ (curve 1); oscillating hole states with $k_y l = 1$, $kl = 2.5$ (both k'_x and q'_x are imagine — curve 2) and $k_y l = 0$, $kl = 0.4$ (k'_x is imagine, q'_x is real — curve 3). The SL spectrum parameters are the same to those indicated in panel (a).

Since the left side of this expression is positive (see Eq.(23)) the allowed values of the energy should be negative if $V > 0$ and *vice versa*. It is not difficult to show that the inequalities (23) and (25) have the solutions when Δ and V differ from zero, $\Delta > |V|$, and $k_y^2 < \Delta^2(\Delta^2 - V^2)/(\hbar v_F V)^2$.

As a result, at $V > 0$ interface states can be realized exclusively inside the hole miniband, while the electron miniband consists of oscillating states only, whose wave functions oscillate, at least, within $0 < x < a$. In Fig.5(a) the hole miniband of the SL with $a = l/2 = 30$ nm is plotted for $V = 11$ meV, $\Delta = 22$ meV, and $k_y l = 1$. Upper narrow slice of the valence miniband depicted by solid line is formed by the interface states. Indeed, it is possible to verify that any energy value from this range obey the inequalities (23) and (25) for the above parameters. Dashed (red) line in the figure shows the interface energy level $|E| = \hbar v_F |k_y| (1 - V^2/\Delta^2)^{1/2}$ for an isolated heterojunction.³⁶

Fig.5(b) represents the squared absolute values of the hole wave functions corresponding to the valence miniband whose profile is shown in Fig.5(a) at $k_y l = 1$. We plot the probability density for some interface state (curve 1) with the energy belonging to the top slice of the valence miniband (solid line in panel (a)). It is seen that $|\Psi(x)|^2$ exponentially drops towards the interface $x = a$. For comparison, in Fig.5(b) we plot also the probability densities for two other states from the valence miniband (curves 2 and 3) oscillating inside the gapless region $0 < x < a$. Solving the Dirac equation at $k_y = 0$ it is not difficult to show that $|\Psi(x)|^2$ is always constant within the gapless region (curve 3). Note also, that in this case the probability density must be symmetric with respect to the points $x = a/2$ and $x = (l + a)/2$, as shown in the

figure.

V. CONCLUDING REMARKS

We have considered the simple model of a one-dimensional SL in which the gap and potential profile are piecewise constant functions. In the framework of this model the dispersion relation for Dirac electrons was obtained, and the structure of low-energy minibands was investigated depending on the potential V and other parameters of the SL.

It was found that beginning with some critical value V_c of the relative band shift V the new contact or cone-like Dirac points appear in the SL spectrum. As a result, at $V > V_c$ the SL becomes gapless. The contact point exists only at certain $V = V_n$ but always at $k = k_y = 0$, while the cone-like points are situated symmetrically related to $k_y = 0$ at some finite $k_y = \pm k_{yn}$ when $V > V_c$. In the case where the widths of the gapless and gapped graphene strips in the SL are equal, we found the positions of the Dirac points in \mathbf{k} -space and obtained an expression for the threshold potential value V_c corresponding to their appearance. The dispersion relation and carrier velocities were analyzed in the vicinity of the contact and cone-like Dirac points.

Appearance of new Dirac points at $k_y \neq 0$ is typical as well for SL induced by the potential modulation of a gapless graphene.^{15–17,33,37} Thus, one may conclude that such a reconstruction of the electron spectrum in a certain extent represents a universal property of graphene-based superlattices.

It should be noted that the description of the SL energy spectrum in our work was carried out within the framework of a one-electron picture. Recent theoretical^{38–40} and experimental^{41–43} investigations of many-particle problem in graphene show that one of the most important consequences of the electron-electron interaction can be the Fermi velocity renormalization. Such a renormalization, presumably, results in different values of v_F in gapless⁴⁰ and gapped⁴⁴ graphene fractions, which should, of course, modify the basic dispersion relation [Eq.(9)]. Nevertheless, there are no yet any rigorous quantitative estimations of the renormalization effect, and experimentally obtained value of v_F is usually close to 10^8 cm/s. Here, we performed our calculations assuming the difference in v_F -values in both graphene fractions to be negligibly small.

Finally, we found that the interface states can exist in the gap-induced SL at certain conditions.

VI. ACKNOWLEDGMENTS

This work was supported by the Russian Foundation for Basic Research (Grants No 11-02-00960 and 13-02-00784) and Russian Ministry of Education and Science (Contract No 07.514.11.4147).

-
- ¹ A.H. Castro Neto, F. Guinea, N.M.R. Peres, K.S. Novoselov, and A.K. Geim, *Rev. Mod. Phys.* **81**, 109 (2009).
- ² O. Klein, *Z. Phys.* **53**, 157 (1929).
- ³ M.I. Katsnelson, K.S. Novoselov, and A.K. Geim, *Nature Phys.* **2**, 620 (2006).
- ⁴ G.M. Maksimova, V.Ya. Demikhovskii, and E.V. Frolova, *Phys. Rev. B* **78**, 235321 (2008); T.M. Rusin and W. Zawadzki, *Phys. Rev. B* **80**, 045416 (2009).
- ⁵ A.K. Geim and K.S. Novoselov, *Nat. Matter* **6**, 183 (2007).
- ⁶ A. De Martino, L. Dell Anna, and R. Egger, *Phys. Rev. Lett.* **98**, 066802 (2007).
- ⁷ G. Giavaras, P.A. Maksym, and M. Roy, *J. Phys.: Condens. Matter* **21**, 102201 (2009).
- ⁸ G. Giavaras and F. Nori, *Phys. Rev. B* **85**, 165446 (2012).
- ⁹ G. Giovannetti, P.A. Khomyakov, G. Brocks, P.J. Kelly, and J. van den Brink, *Phys. Rev. B* **76**, 073103 (2007).
- ¹⁰ S. Lebegue, M. Klintonberg, O. Eriksson, and M.I. Katsnelson, *Phys. Rev. B* **79**, 245117 (2009).
- ¹¹ N.M.R. Peres, *J. Phys.: Condens. Matter* **21**, 095501 (2009).
- ¹² G. Giavaras and F. Nori, *Appl. Phys. Lett.* **97**, 243106 (2010); G. Giavaras and F. Nori, *Phys. Rev. B* **83**, 165427 (2011).
- ¹³ C-H. Park, Y-W. Son, L. Yang, M.L. Cohen, and S.G. Louie, *Nature Phys.* **4**, 213 (2008).
- ¹⁴ C-H. Park, Y-W. Son, L. Yang, M.L. Cohen, and S.G. Louie, *Nano Lett.* **8**, 2920 (2008).
- ¹⁵ C-H. Park, Y-W. Son, L. Yang, M.L. Cohen, and S.G. Louie, *Phys. Rev. Lett.* **103**, 046808 (2009).
- ¹⁶ L. Brey and H.A. Fertig, *Phys. Rev. Lett.* **103**, 046809 (2009).
- ¹⁷ M. Barbier, P. Vasilopoulos, and F.M. Peeters, *Phys. Rev. B* **81**, 075438 (2010).
- ¹⁸ F. Guinea and T. Low, arXiv:1006.0127v1.
- ¹⁹ J.-H. Lee, J.C. Grossman, *Phys. Rev. B* **84**, 113413 (2011).
- ²⁰ L. Dell Anna and A. De Martino, *Phys. Rev. B* **79**, 045420 (2009).
- ²¹ M. Ramezani Masir, P. Vasilopoulos, and F.M. Peeters, *Phys. Rev. B* **79**, 035409 (2009).
- ²² L. Xu, J. An, and C.-D. Gong, *Phys. Rev. B* **81**, 125424 (2010).
- ²³ V.Q. Le, C.H. Pham, and V.L. Nguyen, *J. Phys.: Condens. Matter* **24**, 345502 (2012).
- ²⁴ S. Marchini, S. Günther, and J. Wintterlin, *Phys. Rev. B* **76**, 075429 (2007).
- ²⁵ A.L. Vázquez de Parga, F. Calleja, B. Borca, M.C.G. Passeggi, Jr., J.J. Hinarejos, F. Guinea, and R. Miranda, *Phys. Rev. Lett.* **100**, 056807 (2008).
- ²⁶ P.W. Sutter, J.I. Flege, and E.A. Sutter, *Nature Mater.* **7**, 406 (2008).
- ²⁷ D. Martocchia, P.R. Willmott, T. Brugger, M. Björck, S. Günther, C.M. Schlepütz, A. Cervellino, S.A. Pauli, B.D. Patterson, S. Marchini, J. Wintterlin, W. Moritz, and T. Greber, *Phys. Rev. Lett.* **101**, 126102 (2008).
- ²⁸ H. Yan, Z.-D. Chu, W. Yan, M. Liu, L. Meng, M. Yang, Y. Fan, J. Wang, R.-F. Dou, Y. Zhang, Z. Liu, J.-C. Nie, and L. He, arXiv:1209.1689.
- ²⁹ P.V. Ratnikov, *JETP Lett.* **90**, 469 (2009).
- ³⁰ P.V. Ratnikov and A.P. Silin, *JETP* **114**, 512 (2012).
- ³¹ P. Strange, *Relativistic Quantum Mechanics* (section 9.4), Cambridge University Press 1998.
- ³² B.H.J. McKellar and G.J. Stephenson, *Phys. Rev. A* **36**, 2566 (1987).
- ³³ D.P. Arovas, L. Brey, H.A. Fertig, E.-A. Kim, and K. Zeigler, *New Journal of Physics* **12**, 123020 (2010).
- ³⁴ M. Barbier, F.M. Peeters, P. Vasilopoulos, and J.M. Pereira, *Phys. Rev. B* **77**, 115446 (2008).
- ³⁵ The author of Ref.29 asserts that the minigap can several times exceed the gap value 2Δ .
- ³⁶ P.V. Ratnikov and A.P. Silin, *Physics of the Solid State* **52**, 1763 (2010).
- ³⁷ J.H. Ho, Y.H. Chiu, S.J. Tsai, and M.F. Lin, *Phys. Rev. B* **79**, 115427 (2009).
- ³⁸ V. Kotov, B. Uchoa, V.M. Pereira, A.H.C. Neto, and F. Guinea, *Rev. Mod. Phys.* **84**, 1067 (2012).
- ³⁹ B. Uchoa, J.P. Reed, Yu Gan, Young II Joe, E. Fradkin, P. Abbamonte, and D. Gasa, *Physica Scripta* **146**, 014014 (2012).
- ⁴⁰ J. González, F. Guinea, and M.A.H. Vozmediano, *Nucl. Phys. B* **424** [FS], 595 (1994).
- ⁴¹ A. Luican, G. Li, and E.Y. Andrei, *Phys. Rev. B* **83**, 041405 (2011).
- ⁴² D.C. Elias, R.V. Gorbachev, A.S. Mayorov, S.V. Morozov, A.A. Zhukov, P. Blake, L.A. Ponomarenko, I.V. Grigorieva, K.S. Novoselov, F. Guinea, *et al.*, *Nature Phys.* **7**, 701 (2011).
- ⁴³ D.A. Siegel, C. Park, C. Hwang, J. Deslippe, A.V. Fedorov, S.G. Louie, and A. Lanzara, *PNAS* **108**, 11365 (2011).
- ⁴⁴ A. Sinner and K. Ziegler, *Phys. Rev. B* **82**, 165453 (2010).